Hydrovolcanic Explosions at the Lava Ocean Entry of the 2018 Kilauea Eruption Recorded by Ocean-Bottom Seismometers

Puja Banerjee*[1] and Yang Shen[1]

Abstract

From the beginning of May 2018, the Kilauea Volcano on the island of Hawaii experienced its largest eruption in 200 yr followed by a period of unrest for months. Because hot molten lava entered the ocean from the ocean-entry point near the lower East Rift Zone, the lava–water interaction led to explosions. Some explosions were near the water surface and ejected fragments of lava, also known as lava bombs. In the early morning on 16 July 2018, one of those lava bombs, which was almost the size of a basketball, hit a sightseeing boat and injured 23 people. In this study, we analyzed the hydrophone data recorded from July to mid-September by ocean-bottom seismometers (OBSs) deployed offshore near the ocean entry point to identify and locate the hydroacoustic signals of the lava–water explosions. Acoustic signals of hydrovolcanic explosions are characterized by a short duration (less than a few seconds) and a broad frequency range (at least up to 100 Hz). To automate event detection, a short-term average versus long-term average method was applied to the complete dataset. Approximately 4300 events were detected and located near the coastline and further used to prepare a catalog. The distribution of the lava–water explosions is consistent with the pattern of the offshore lava delta formed during the 2018 eruption. Identifying such hydroacoustic signals recorded by OBSs may provide new avenues of research using various seismoacoustic events associated with volcanic eruptions.

Cite this article as Banerjee, P., and Y. Shen (2023). Hydrovolcanic Explosions at the Lava Ocean Entry of the 2018 Kilauea Eruption Recorded by Ocean-Bottom Seismometers, *Seismol. Res. Lett.* **94**, 1488–1494, doi: 10.1785/0220220195.

Supplemental Material

Introduction

Interactions between hot molten lava and cold seawater give rise to hydrovolcanic explosions, also known as *littoral explosions* in the related literature (e.g., Moore and Ault, 1965; Sansone *et al.*, 1991; Mattox and Mangan, 1997; Haxel and Dziak, 2005; Schlindwein and Riedel, 2010; Tan *et al.*, 2016; Le Saout *et al.*, 2020; Tepp and Dziak, 2021). The dynamics of the interactions are complex, and our understanding is often limited because of the lack of direct observations from the volcanic eruption. Factors limiting our understanding of the interactions include remote and hazardous conditions near the explosions, few geophysical sensors, nonuniform lava-flow morphology, and variations in sound speed profiles. Nevertheless, investigations on lava–water interactions in the mid-oceanic ridge settings, captured by different instruments such as automated underwater vehicles and remote sensing, have been carried out to constrain the physical factors such as fluxes, lava volume, flow rates, types of lava flows, grain size, and the intensity of explosions (Fröhlich *et al.*, 1993; Caplan-Auerbach *et al.*, 2017; Le Saout *et al.*, 2020; Dietterich *et al.*, 2021).

Kilauea is an active volcano on the island of Hawaii where for over decades erupted lava flows have entered the ocean (Sansone *et al.*, 1991; Mattox and Mangan, 1997). This interaction has allowed studies of different aspects of the lava–water explosions (e.g., Mattox and Mangan, 1997; Caplan-Auerbach and Duennebier, 2001; Caplan-Auerbach *et al.*, 2001). The 2018 Kilauea Volcano eruption was the most destructive eruption on the island in the past 200 years (Klein, 1982; Neal *et al.*, 2019; Patrick *et al.*, 2020). In April 2018, Kilauea's Halemaʻumaʻu crater was 200 m wide before the onset of the major eruption. Dike intrusion in the lower East Rift Zone (LERZ) triggered a major earthquake of M_w 6.9 offshore followed by caldera collapse and intense magmatism (Chen *et al.*, 2019; Neal *et al.*, 2019; Dietterich *et al.*, 2021). During the eruption, lava flow entered the ocean from the LERZ, leading to hydrovolcanic explosions, as well as adding 3.5 km^2 of new land to the island and 0.76 km^3 of lava deltas offshore (Neal *et al.*, 2019; Dietterich *et al.*, 2021; Soule *et al.*, 2021).

1. Graduate School of Oceanography, The University of Rhode Island, Narragansett, Rhode Island, U.S.A., https://orcid.org/0000-0002-4185-6089 (YS)

*Corresponding author: puja_banerjee@uri.edu

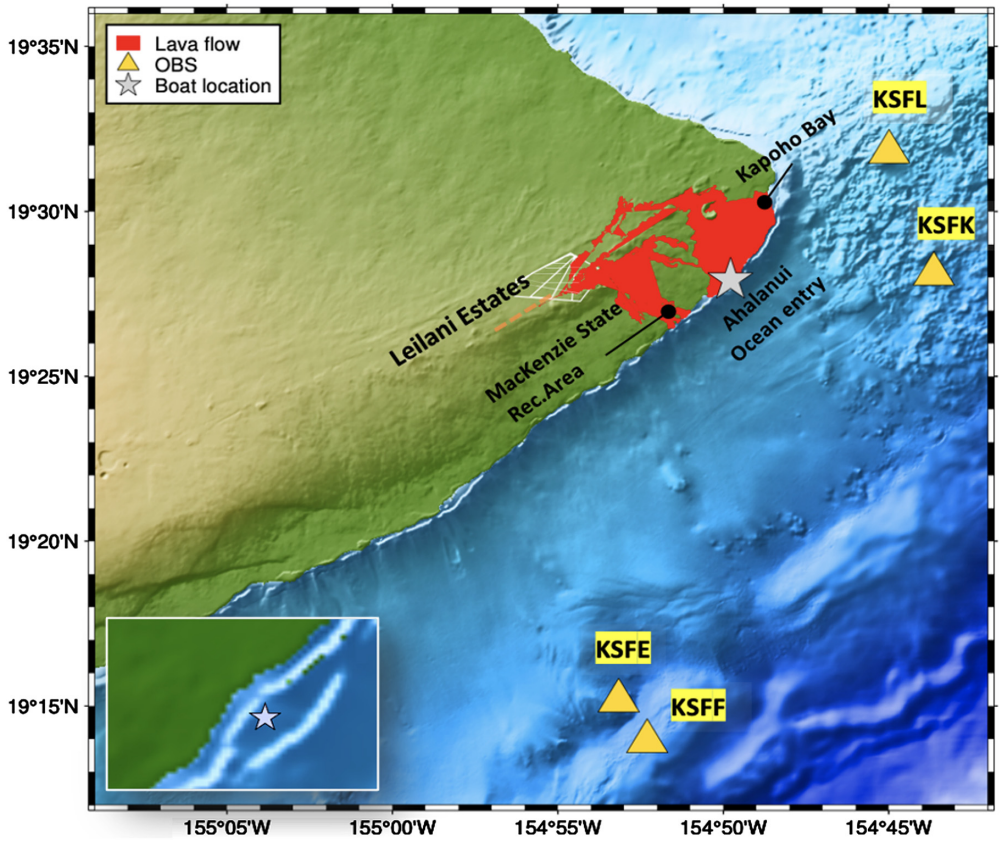

Figure 1. Map of the lava flows of the 2018 Kilauea volcanic eruption, which is shown in red (Zoeller *et al.*, 2020). Lava flows from the eruption also covered parts of the Leilani Estates. The gray star indicates the location of the tour boat when it was hit by the lava bomb near the coastline. The four yellow triangles are the ocean-bottom seismometers deployed closest to the active ocean entry used in our analysis. (Inset) The tour boat's location relative to the ocean entry. The color version of this figure is available only in the electronic edition.

According to the accounts of the eruption (Neal *et al.*, 2019; Patrick *et al.*, 2020), as the caldera collapsed, magma supply from the volcano kept flowing toward Kapoho Bay between mid-May to the end of June. In early July, the flow changed its course as it moved toward the Ahalanui region. This active ocean entry served as a hotspot for the lava–water explosions. To record the seismicity beneath the submarine south flank of Kilauea and the lava–water interactions near the lava ocean entry located in the southeastern flank of the volcano, 12 short-period ocean-bottom seismometers (OBSs) with a sampling rate of 200 Hz were deployed offshore on 10 July 2018, soon after the lava flows started pouring over the coastline (Wei *et al.*, 2021). Eleven OBSs were recovered on 16 September after the eruption stopped. The OBSs had three-component geophone channels (EL1, EL2, and ELZ) and a hydrophone channel (EDH) that recorded the hydroacoustic signals associated with the lava–water explosions near the shoreline (Caplan-Auerbach *et al.*, 2019; Wei *et al.*, 2021).

This study detects and characterizes lava–water interactions in terms of hydroacoustic signals from the hydrophone channels of the OBSs to generate a catalog of lava–water explosions and to understand their relationship to lava delta deposits. Inspection of the hydrophone records showed that the four OBSs closest to the lava ocean entry (Fig. 1; KSFL, KSFK, KSFE, and KSFF) best captured the acoustic signals from the lava–water explosions, whereas those farther away from the ocean entry had a much lower signal-to-noise ratio. We therefore focused the analysis of hydroacoustic signals on the four OBSs closest to the lava ocean entry.

Hydrophone Data and Detection of Hydroacoustic Explosions

Acoustic data recorded by hydrophones are a great source for studying volcanic activities near ocean entry. In shallow water, lava–water interactions may lead to explosions that eject chunks of molten or semi-solidified lava, which are known as "lava bombs" and are a clear hazard. On 16 July 2018, one such incident happened in the early morning when a lava bomb, almost the size of a basketball, hit a sightseeing tour boat near the lava ocean entry south of the LERZ (Fig. 1) and injured 23 people (details are provided in Text S1, available in the supplemental material to this article). According to a witness account, the tour boat was within ~250 m of the lava ocean-entry point at the time of the incident, which was a substantial excursion from its recommended route. Because the tour boat location was in close proximity to the lava ocean entry point, we assume that the lava bomb origin location was in close proximity to the tour boat's location (this is verified subsequently), and any offset is within our margin of error (~200 m).

To estimate the lava bomb origin, we started with identifying the explosion signal in the hydrophone channels, considering the event that hit the tour boat. To identify the lava bomb signal, we used the ground truth time and location from the metadata embedded in the cell phone pictures captured by a passenger on the tour boat on her smartphone as a

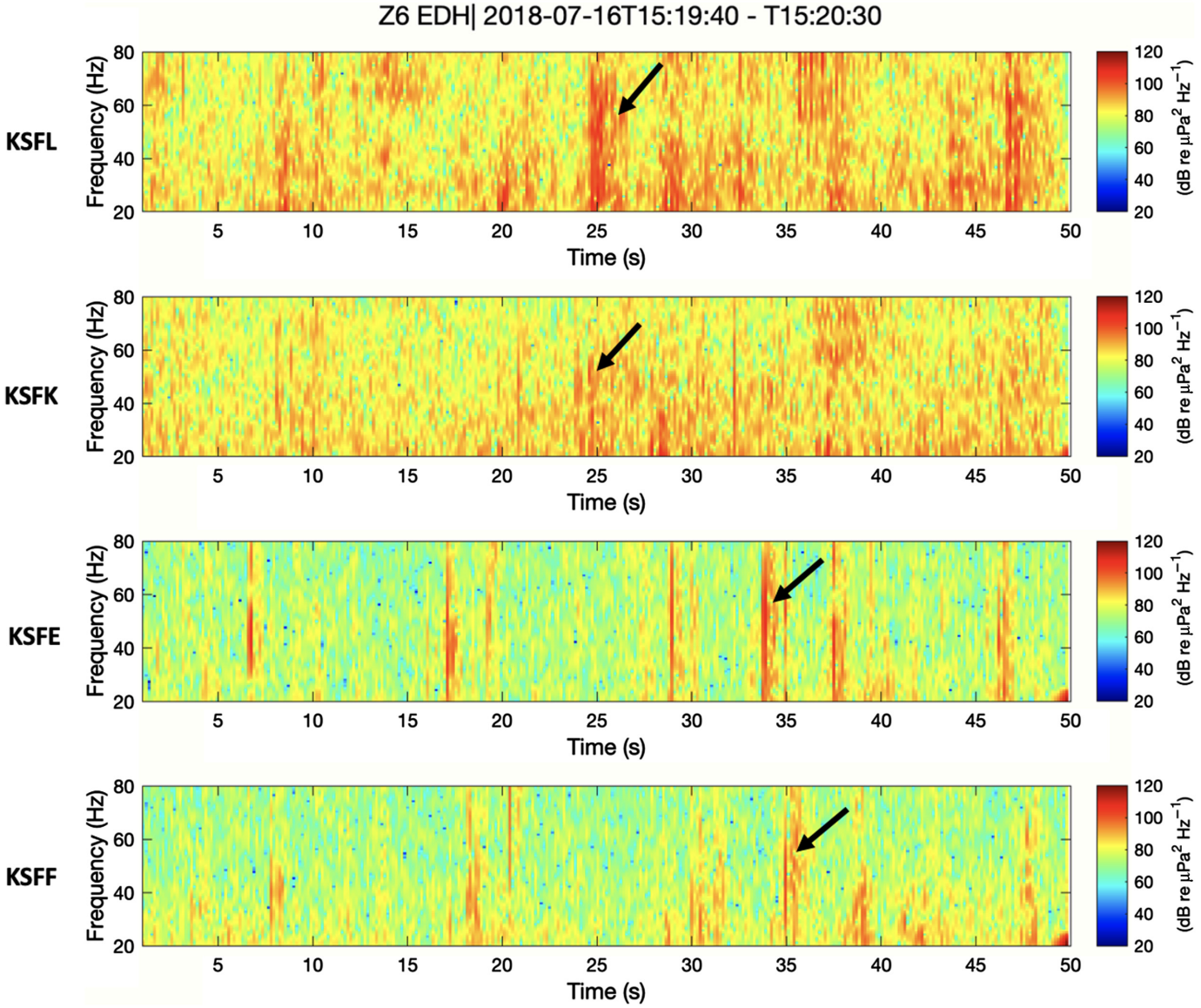

reference (see Text S2). Hydrovolcanic explosions can be characterized by a broad frequency range between 20 and 80 Hz and a very short duration (<~2–3 s). Spectrograms (Fig. 2) show the hydroacoustic data within a 50 s time window surrounding the time of the lava bomb incident (as observed from phone's metadata) in the four hydrophone EDH channels. Hydrophone channel data were recorded with a sampling rate of 200 Hz. These data were bandpass filtered between 20 and 80 Hz to enhance hydrovolcanic explosion signals and reduce those generated by ground motion or seismic noise.

After manually identifying the event in multiple hydrophone channel recordings and noting their arrival times, we picked the signals at each station and used them to determine the event location (see Text S3 for details). The location was found to be within ~190 m from the tour boat's location, confirming that we identified the correct signals for the explosion. Because of the complexity and variability of waveforms, we calculated the arrival delay times between the four station (KSFE, KSFF, KSFK, and KSFL) pair combinations by picking the "peak" values of the power envelopes (see Text S3) from their associated windowed waveforms. Because the OBSs were deployed at different depths (Wei

Figure 2. Spectrograms are shown for a 50 s window (UTC 15:19:40–15:20:30, which is around 5:20 a.m. HST) for the hydrophone component of the four stations. The spectrograms are calculated with nonequispaced fast Fourier transform (60 samples, default 50% overlap). Lava–water explosion signals are high-energy, short-duration, and broad-frequency signals seen throughout the spectrograms ranging between 20 to 80 Hz. The arrow points to the identified explosion signal of the lava bomb that hit the tour boat. The time lag in the identified signal is caused by varying arrival times from the explosion site to each station. The color version of this figure is available only in the electronic edition.

et al., 2021), the station locations and depths were crucial to calculating the differential travel times between each station pair. The delay times between different station pairs were also calculated using the triangulation method by including both the location as well as its depth and assuming a constant sound velocity of 1.5 km/s (del Pezzo *et al.*, 2002; Caplan-Auerbach *et al.*, 2017; Metz *et al.*, 2018) and compared with the values obtained from the peaks of the power envelopes. Finally, the source location was estimated by performing a grid-search evaluation (with a spacing of 200 m) along the coastline using MATLAB, with a least-square misfit to the differential travel times.

Using the determined signal characteristics, we developed a catalog of explosions for the period of OBS deployment. Automated detection of seismic or acoustic events in a noisy environment is challenging (Vaezi and Van der Baan, 2015). A commonly used method to detect seismic events is short-term average versus long-term average (STA/LTA), a trigger algorithm that detects signals from a continuous dataset with preset values of the moving windows (Allen, 1982; Withers *et al.*, 1998; Trnkoczy, 2012). On the hydrophone data band-pass-filtered between 20 and 80 Hz, this STA/LTA method was applied to automate the detection of lava–water explosion signals. The algorithm parameters were set via trial and error and visual inspection of the results, with 5 s as the maximum time window size (LTA) and 1 s as the short window size (STA) (see Text S4; Fig. S4). An event is labeled when the STA/LTA ratio is larger than 4. This STA/LTA detector was applied to the complete span of the two-month dataset for screening hydrovolcanic explosions for each station. Each station has thousands of local detections (Table S1). However, to locate the events and better constrain their relationship with the offshore lava deposit, we associate all the four stations' common detections that are within ∼1 s, after accounting for the propagation time to a single event in the catalog, using the least-square travel-time misfit. The event's source location uncertainties (root-mean-square error) were also calculated, keeping in mind the limitations due to travel-time misfit and picking errors and a constant sound velocity of 1.5 km/s. The root-mean-square magnitude, that is, inverse square law approximation, to estimate the magnitude at the receiver location (received level or RL_{rms}) of each event was also calculated in decibels from each signal considering a constant sound speed in the water column and by using the travel-time arrivals from the events to the station KSFK (Greinert and Nützel, 2004; Farcas *et al.* 2016; Tan *et al.*, 2016; Crone and Bohnenstiehl, 2019). The magnitude was measured over a fixed 1 s window for the filtered frequency range around the event time.

Results

The final catalog includes the event location (point of origin near the coastline), origin time, least-square error estimations associated with the location, and calculated magnitude. Approximately 4300 events were detected and located over the active eruption phase between 11 July 2018 and 4 August 2018, when the fissure eruption stopped. Our catalog has the highest density of explosion records near the Ahalanui ocean entry with ∼1200 events (Fig. 3a), which served as the hotspot beginning from mid-July until the end of eruption (Dietterich *et al.*, 2021; Soule *et al.*, 2021). The spatiotemporal event distribution of the binned events (per 0.5 km distance) has the highest count of ∼145 events in a day (23 July), as shown in Figure 4a. The daily event counts show a brief quiet period after 23 July 2018, possibly because of a hiatus in the rate of lava ocean entry or background noise.

In the catalog, we also observe that the magnitude of events varies from 130.6 to 197.4 dB re 1 μPa, with the median and maximum magnitudes decreasing toward the end (Fig. 4b,c; Fig. S5). The highest magnitude explosions were mostly located near the Ahalanui ocean entry, where hotter lava volumes were deposited because of a fresh supply of magma during this eruption phase (Dietterich *et al.*, 2021). The identified hydrovolcanic explosion signal of the lava bomb that hit the tour boat has an estimated magnitude of ∼151 dB, not the strongest, because the catalog contains many other higher magnitude events.

Discussion and Conclusions

The 2018 eruption of Kilauea led to the opening of several fissures, resulting in high volumes of lava reaching the coastline. According to Hawaiian Volcano Observatory (HVO) reports, the lava ocean entry at the beginning of eruption in May was concentrated near the Mackenzie State Recreation Area (Fig. 1). By early July, the active lava ocean entry shifted farther to the east, leading to new ocean entry to the south of Ahalanui. Because our OBS deployment was in early July (Wei *et al.*, 2021) near the southeastern flank of Ahalanui, the instruments could monitor activity after 11 July until 16 September. Our catalog has the highest intensity of explosion records near the Ahalanui ocean entry during mid-July and a quick drop in the number of explosion events around 4 August 2018 (Fig. 4a), when the fissure eruption stopped (Neal *et al.*, 2019; Dietterich *et al.*, 2021). Therefore, our findings are consistent with the chronology of the eruption events as reported by HVO.

Identified lava-water explosions in our catalog also appeared to match the 2018 lava delta deposits near the coastline to the first order. The lava ocean entry near the MacKenzie State Recreation Area and most of the lava-entry activities northeast of Ahalanui near Kapoho bay (Dietterich *et al.*, 2021; Soule *et al.*, 2021) occurred before the OBS deployment. In the Ahalanui segment, the largest numbers of lava–water explosions correspond to thick lava deposits (≤200 m) and greatest coastline expansion toward the ocean

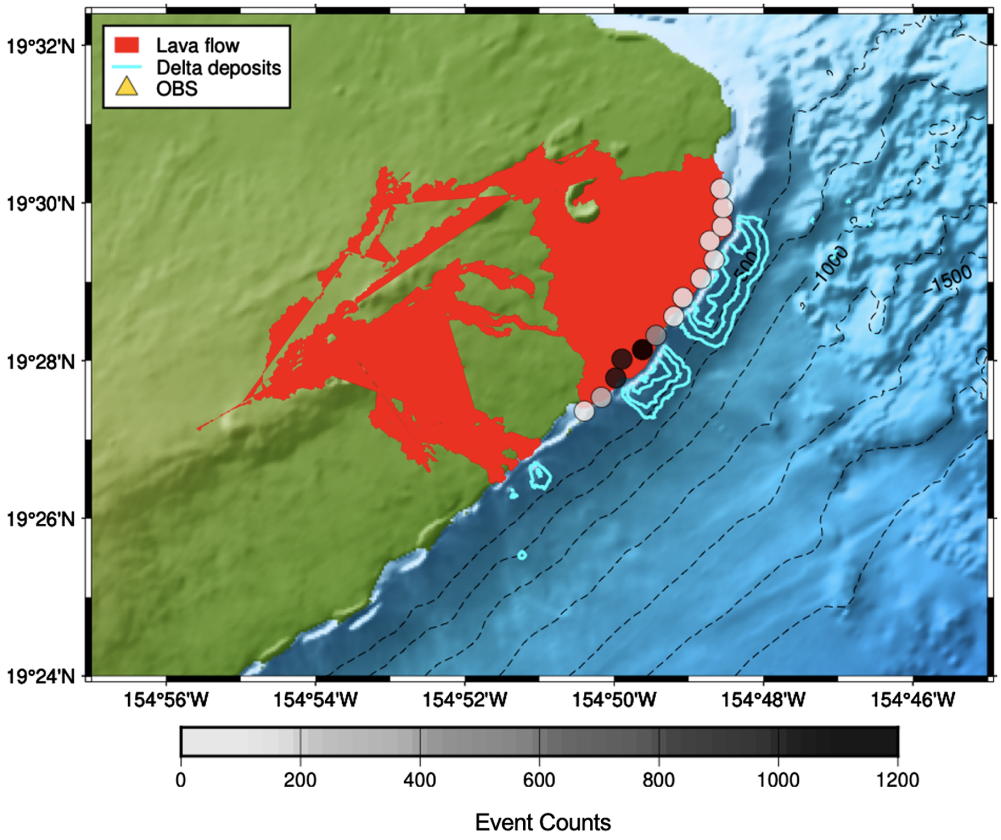

Figure 3. Map illustrating the identified hotspot locations in terms of the number of events near the active ocean entry. The circles are the hydrovolcanic explosions detected along the coastline gridded per 0.5 km of distance (between the two end points at 19.456° N, 154.840° W, and 19.507° N, 154.809° W). The varying shades of circle denote the number of the events within that region. The highest record of detected events was between 19.468° N, 154.829° W, and 19.471° N, 154.825° W. Lava flows reached the coastline leading to delta deposits and change of the coast line (Soule *et al.*, 2021). Cyan blue contours denote the bathymetric change at 50 m intervals that is attributed to the new lava delta deposits formed during the 2018 eruption. The color version of this figure is available only in the electronic edition.

with a higher slope (~20°–35°) of contact as shown in Figure 3.

Hydrovolcanic explosions at the lava ocean entry have distinct hydroacoustic signatures than other acoustic signals such as landslides or bench collapses (Caplan-Auerbach *et al.*, 2001, 2017; Tan *et al.*, 2016; Tepp and Dziak, 2021), which are characterized by much longer durations (Figs. S2 and S6). A future study of the relationships between hydrovolcanic explosions and landslides or bench collapses may provide additional insights into the dynamics of lava–water interaction as well as better understanding of related hazards.

Our catalog provides useful insights on the continuous hydroacoustic monitoring of volcanic eruptions, which can possibly be used for hazard assessment and warning by the hazard monitoring agencies. The catalog (attached with the supplemental material) may also be used to facilitate studies of the seismic and infrasound signals of hydrovolcanic explosions (Wang *et al.*, 2021; Thelen *et al.*, 2022). Further studies on the temporal variation of erupted lava volume flowing downstream from the fissure to the ocean entry could provide additional support to the variations in the explosion frequency over time. Observations from hydroacoustic research may provide new avenues for studying volcanic eruptions, submarine landslides, bench collapses, and other coastal volcanic processes.

Data and Resources

All the hydroacoustic data of this study are publicly available from the Incorporated Research Institute for Seismology Data Management Center under the network code Z6 (Caplan-Auerbach *et al.*, 2018). The supplemental material includes text, eight figures, and two tables, providing an important and detailed description of our analysis, which was used to generate event catalog. The catalog (.txt file) is also attached along with the supplemental material. All the analysis was done using ObsPy (Beyreuther *et al.*, 2010), and maps were prepared using Generic Mapping Tools version 6 (Wessel *et al.*, 2019).

Declaration of Competing Interests

The authors declare there are no competing interests.

Acknowledgments

The authors are grateful to Laci Stanton, a passenger on the tour boat that was hit by a lava bomb, who shared her experience and pictures and videos of the event, which were very useful in this study. The authors thank Gopu Potty for his constructive reviews on hydroacoustic concepts and ray path modeling that helped us to improve this article. The authors also thank Adam Soule for sharing the bathymetry file for lava delta deposits data. The authors thank the crews and the scientific parties of the KOK1805 and MGL1806 cruises for the ocean-bottom seismometer deployment and recovery. Constructive feedback from Gabrielle Tepp and D. R. Bohnenstiehl helped improve this article. This study is funded by National Science Foundation Grant Number 1949620.

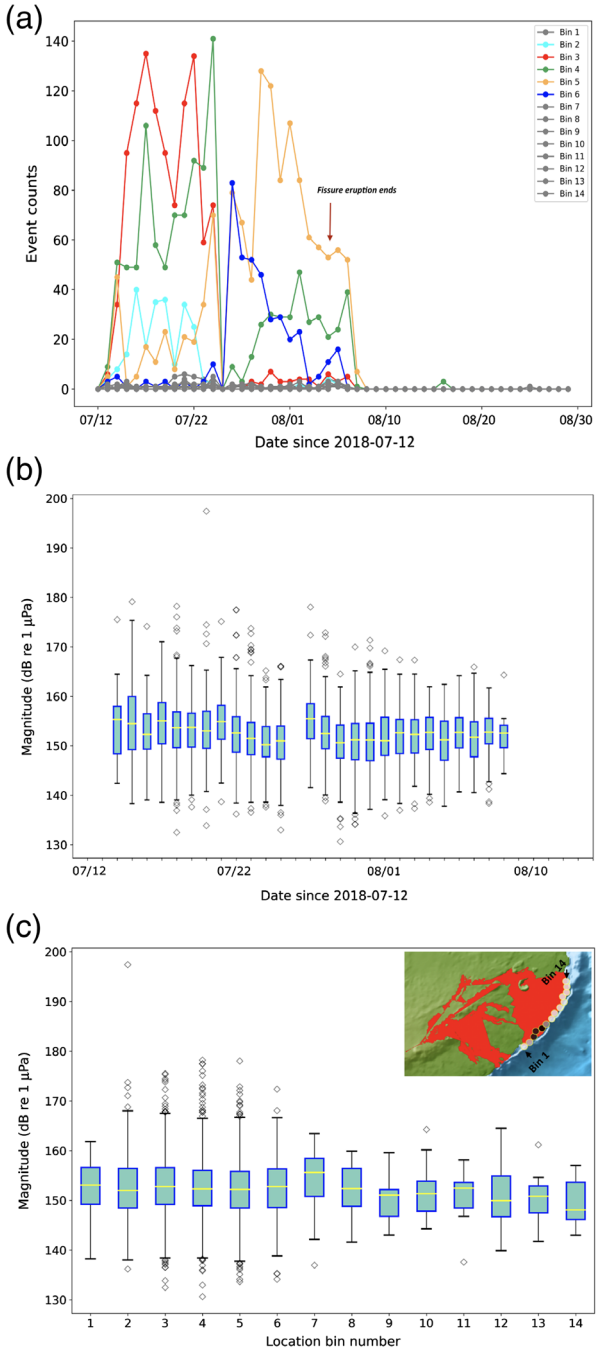

Figure 4. (a) Daily distribution of detected events in the catalog from 12 July 2018 to 30 August 2018. The bin numbers are in sequence from bottom left to the top right (between 19.456° N, 154.840° W, and 19.507° N, 154. 809° W) as shown in the inset of panel (c). (b) The temporal variation in the calculated magnitude of the events shown for the most active phase of eruption before fissure eruption ends on 4 August 2018. (c) Spatial magnitude variation across the binned locations. In panels (b,c), the boxplot represents the quantitative magnitude distribution. The whiskers (in black) denote the upper and lower quartiles of the distribution. The yellow line is the median of the spread, and the outliers (diamond shapes) are the extreme magnitudes that do not fall within the upper and lower quartiles. The color version of this figure is available only in the electronic edition.

References

Allen, R. (1982). Automatic phase pickers: Their present use and future prospects, *Bull. Seismol. Soc. Am.* **72,** no. 6B, S225–S242, doi: 10.1785/BSSA07206B0225.

Beyreuther, M., R. Barsch, L. Krischer, T. Megies, Y. Behr, and J. Wassermann (2010). ObsPy: A Python toolbox for seismology, *Seismol. Res. Lett.* **81,** no. 3, 530–533.

Caplan-Auerbach, J., and F. Duennebier (2001). Seismic and acoustic signals detected at Loihi Seamount by the Hawaii Undersea Geo-Observatory, *Geochem. Geophys. Geosys.* **2,** doi: 10.1029/2000GC000113.

Caplan-Auerbach, J., R. P. Dziak, J. Haxel, D. R. Bohnenstiehl, and C. Garcia (2017). Explosive processes during the 2015 eruption of Axial Seamount, as recorded by seafloor hydrophones, *Geochem. Geophys. Geosys.* **18,** no. 4, 1761–1774, doi: 10.1002/2016GC006734.

Caplan-Auerbach, J., C. G. Fox, and F. K. Duennebier (2001). Hydroacoustic detection of submarine landslides on Kilauea Volcano, *Geophys. Res. Lett.* **28,** no. 9, 1911–1833, doi: 10.1029/2000GL012545.

Caplan-Auerbach, J., J. K. Morgan, and Y. Shen (2018). OBS survey of Kilauea's submarine south flank following the May 4, 2018 M6.9 earthquake and lower East Rift Zone eruption [Dataset], *International Federation of Digital Seismograph Networks*, 10.7914/SN/Z6_2018.

Caplan-Auerbach, J., Y. Shen, J. Morgan, and S. A. Soule (2019). Hydroacoustic recordings of lava-water interactions and landslides during the 2018 eruption of Kilauea Volcano, *2019 Fall AGU meeting*, abstract V41A-01.

Chen, K., J. D. Smith, J.-P. Avouac, Z. Liu, Y. T. Song, and A. Gualandi (2019). Triggering of the Mw 7.2 Hawaii earthquake of 4 May 2018 by a dike intrusion, *Geophys. Res. Lett.* **46,** no. 5, 2503–2510, doi: 10.1029/2018GL081428.

Crone, T. J., and D. R. Bohnenstiehl (2019). Acoustic evidence of a long-lived gas-driven submarine volcanic eruption in the Bismarck Sea, *Geophys. J. Int.* **217,** no. 1, 169–178, doi: 10.1093/gji/ggy542.

del Pezzo, E., A. Esposito, F. Giudicepietro, M. Marinaro, M. Martini, and S. Scarpetta (2002). Seismological discrimination of earthquakes and underwater explosions using neural networks: An application to volcanic monitoring, *EGS General Assembly Conference Abstracts*, 4273, doi: 10.1785/0120020005.

Dietterich, H. R., A. K. Diefenbach, S. A. Soule, M. H. Zoeller, M. P. Patrick, J. J. Major, and P. R. Lundgren (2021). Lava effusion rate evolution and erupted volume during the 2018 Kīlauea lower East Rift Zone eruption, *Bull. Volcanol.* **83,** no. 4, doi: 10.1007/s00445-021-01443-6.

Farcas, A., P. M. Thompson, and N. D. Merchant (2016). Underwater noise modelling for environmental impact assessment, *Environ. Impact Assess. Rev.* **57,** 114–122, doi: 10.1016/j.eiar.2015.11.012.

Fröhlich, G., B. Zimanowski, and V. Lorenz (1993). Explosive thermal interactions between molten lava and water, *Exp. Therm Fluid Sci.* **7,** no. 4, 319–332, doi: 10.1016/0894-1777(93)90055-N.

Greinert, J., and B. Nützel (2004). Hydroacoustic experiments to establish a method for the determination of methane bubble fluxes at cold seeps, *Geo-Mar. Lett.* **24,** no. 2, 75–85, doi: 10.1007/s00367-003-0165-7.

Haxel, J. H., and R. P. Dziak (2005). Evidence of explosive seafloor volcanic activity from the Walvis ridge, South Atlantic Ocean, *Geophys. Res. Lett.* **32,** L13609, doi: 10.1029/2005GL023205.

Klein, F. W. (1982). Patterns of historical eruptions at Hawaiian volcanoes, *J. Volcanol. Geotherm. Res.* **12,** no. 1, 1–35, doi: 10.1016/0377-0273(82)90002-6.

Le Saout, M., D. R. Bohnenstiehl, J. B. Paduan, and D. A. Clague (2020). Quantification of eruption dynamics on the north rift at Axial Seamount, Juan de Fuca ridge, *Geochem. Geophys. Geosys.* **21,** no. 9, doi: 10.1029/2020GC009136.

Mattox, T. N., and M. T. Mangan (1997). Littoral hydrovolcanic explosions: A case study of lava–seawater interaction at Kilauea Volcano, *J. Volcanol. Geotherm. Res.* **75,** nos. 1/2, 1–17, doi: 10.1016/S0377-0273(96)00048-0.

Metz, D., A. B. Watts, I. Grevemeyer, and M. Rodgers (2018). Tracking submarine volcanic activity at Monowai: Constraints from long-range hydroacoustic measurements, *J. Geophys. Res.* **123,** no. 9, 7877–7895, doi: 10.1029/2018JB015888.

Moore, J. G., and W. U. Ault (1965). Historic littoral cones in Hawaii, *Pac. Sci.* **9,** 3–11.

Neal, C. A., S. R. Brantley, L. Antolik, J. L. Babb, M. Burgess, K. Calles, M. Cappos, J. C. Chang, S. Conway, L. Desmither, *et al.* (2019). The 2018 rift eruption and summit collapse of Kīlauea Volcano, *Science* **363,** no. 6425, 367–374, doi: 10.1126/science.aav7046.

Patrick, M. R., B. F. Houghton, K. R. Anderson, M. P. Poland, E. Montgomery-Brown, I. Johanson, W. Thelen, and T. Elias (2020). The cascading origin of the 2018 Kīlauea eruption and implications for future forecasting, *Nat. Commun.* **11,** no. 1, 5646, doi: 10.1038/s41467-020-19190-1.

Sansone, F. J., J. A. Resing, G. W. Tribble, P. N. Sedwick, K. M. Kelly, and K. Hon (1991). Lava-seawater interactions at shallow-water submarine lava flows, *Geophys. Res. Lett.* **18,** no. 9, 1731–1734, doi: 10.1029/91GL01279.

Schlindwein, V., and C. Riedel (2010). Location and source mechanism of sound signals at Gakkel ridge, Arctic Ocean: Submarine Strombolian activity in the 1999–2001 volcanic episode, *Geochem. Geophys. Geosys.* **11,** doi: 10.1029/2009GC002706.

Soule, S. A., M. Zoeller, and C. Parcheta (2021). Submarine lava deltas of the 2018 eruption of Kīlauea Volcano, *Bull. Volcanol.* **83,** no. 4, doi: 10.1007/s00445-020-01424-1.

Tan, Y. J., M. Tolstoy, F. Waldhauser, and W. S. D. Wilcock (2016). Dynamics of a seafloor-spreading episode at the East Pacific Rise, *Nature* **540,** no. 7632, 261–265, doi: 10.1038/nature20116.

Tepp, G., and R. P. Dziak (2021). The seismo-acoustics of submarine volcanic eruptions, *J. Geophys. Res.* **126,** no. 4, doi: 10.1029/2020JB020912.

Thelen, W., G. Waite, J. Lyons, and D. Fee (2022). Infrasound observations and constraints on the 2018 eruption of Kilauea Volcano, Hawaii, *Bull. Vol.* **84,** doi: 10.1007/s00445-022-01583-3.

Trnkoczy, A. (2012). Understanding and parameter setting of STA/LTA trigger algorithm, *New Manual of Seismological Observatory Practice* (2002), revised version, doi: 10.2312/GFZ.NMSOP-2_IS_8.1.

Vaezi, Y., and M. Van der Baan (2015). Comparison of the STA/LTA and power spectral density methods for microseismic event detection, *Geophys. J. Int.* **203,** no. 3, 1896–1908, doi: 10.1093/gji/ggv419.

Wang, C., Y. Shen, and P. Banerjee (2021). Identifying lava bombs in seismometer data during the 2018 Kilauea eruption, *Abstract V25D-0153 Presented at 2021 Fall AGU Meeting, AGU*, New Orleans, LA, 13–17 December 2021.

Wei, X., Y. Shen, J. Caplan-Auerbach, and J. K. Morgan (2021). An OBS array to investigate offshore seismicity during the 2018 Kīlauea eruption, *Seismol. Res. Lett.* **92,** no. 1, 603–612, doi: 10.1785/0220200206.

Wessel, P., J. F. Luis, L. Uieda, R. Scharroo, F. Wobbe, W. H. Smith, and D. Tian (2019). The Generic Mapping Tools version 6, *Geochem. Geophys. Geosys.* **20,** no. 11, 5556–5564, doi: 10.1029/2019GC008515.

Withers, M., R. Aster, C. Young, J. Beiriger, M. Harris, S. Moore, and J. Trujillo (1998). A comparison of select trigger algorithms for automated global seismic phase and event detection, *Bull. Seismol. Soc. Am.* **88,** no. 1, 95–106, doi: 10.1785/BSSA0880010095.

Zoeller, M., R. Perroy, R. Wessels, G. Fisher, J. Robinson, J. Bard, J. Peters, A. Mosbrucker, and C. Parcheta (2020). Geospatial database of the 2018 lower East Rift Zone eruption of Kīlauea Volcano, Hawaii, *U.S. Geol. Surv. Data Release*, doi: 10.5066/P9S7UQKQ.

Manuscript received 20 June 2022
Published online 8 March 2023